CrystEngComm

Accepted Manuscript

This article can be cited before page numbers have been issued, to do this please use: R. M. Gomila and A. Frontera, *CrystEngComm*, 2020, DOI: 10.1039/D0CE00220H.

ROYAL SOCIETY OF CHEMISTRY

rsc.li/crystengcomm

ROYAL SOCIETY OF CHEMISTRY View Article Online
DOI: 10.1039/D0CE00220H

Journal Name

ARTICLE

Charge assisted halogen and pnictogen bonds: insights from the Cambridge Structural Database and DFT calculations

Received 00th January 20xx,
Accepted 00th January 20xx

DOI: 10.1039/x0xx00000x

www.rsc.org/

Rosa M. Gomila[a] and Antonio Frontera*[b]

This manuscript combines a search in the Cambridge Structural Database (CSD) and theoretical density functional theory (DFT) calculations to analyse the existence and importance of charge assisted pnictogen and halogen bonds involving halophosphonium cations. Trivalent pnictogen atoms typically have three σ-holes and are able to establish up to three pnictogen bonds (PnBs). In phosphonium salts the phosphorus atom forms four covalent bonds and, consequently, four σ-holes are located at the extension of these bonds. Therefore, up to four charge assisted PnBs can be formed between these holes and the counterions or any electron rich atom. The covalent bonds arrangement around the phosphorus atom is similar to tetravalent tetrel atoms and converts into a similar pattern of σ–hole interactions. We have found and described this type of charge assisted pnictogen bonds in various halophosphonium crystal structures. Moreover, the competition of charge assisted PnBs with charge assisted halogen bonds (HaB) has been also studied both theoretically and analysing the CSD.

Introduction

Similarly to hydrogen, elements of the p-block of the periodic table can behave as electrophile and participate in attractive interactions with electron rich sites.[1-6] In these p-block elements, the electron density distribution is normally anisotropic, especially when they are covalently bonded to elements of higher electronegativity, thus presenting both regions of positive and negative electron density.[7-8] The location and number of positive regions (namely σ-holes) is associated with the position and number of the covalent bonds established by the p-block element.[9] That is, the number of σ-holes depends on the number of covalent bonds. For example, halogen, chalcogen, pnictogen and tetrel atoms classically form one, two, three and four covalent bonds and σ-holes may be located opposite to these bonds.[10] These regions of depleted charge typically form highly directional interactions which are named using the name of the p-block group. That is, halogen bond (HaB)[1] for group 17, chalcogen bond (ChB),[11] for group 16, pnictogen bond (PnB)[3,12] for group 15 and tetrel bond (TrB) for group 14.[13,14]

The attention in PnB by the scientific community has increased in recent years.[2,15,16] For instance, triple-pnictogen bonding has been used as a tool for supramolecular assembly[17] and phosphonium–stibonium and bis-stibonium cations has been utilized as pnictogen-bonding catalysts for the hydrogenation of quinolines.[18] Moreover, Matile's group has used pnictogen-bonding interactions for transmembrane anion transport and compared their characteristics with chalcogen- and halogen-bonding analogs.[19] The positive electrostatic potential energy value at the σ holes increases on going from top to bottom of group 15 because the polarizability of the pnicogen atom increases. In fact, pnictogen bonds involving antimony have materialized as the most promising ones for incorporation into functional systems.[20]

The utilization of the heavier pnictogen atoms to establish effective and competitive interaction in solution is a good strategy to succeed in the fields of supramolecular chemistry and catalysis.[21] Another strategy is the utilization of tetravalent phosphorus cations as PnB donor sites ($R_4P^+\cdots$:A). Tetrasubstituted phosphorus atoms should be able to afford particularly strong charge-assisted pnictogen bonds. Moreover, the presence of up to four σ-holes is expected on phosphorus, consequently enabling for up to four PnBs to be established. For chalcogen elements, the formation of three charge assisted chalcogen bonds in sulfur,[22,23] selenium and tellurium has been studied theoretically and analysed using the CSD.[24] Moreover, charge assisted ChBs have been described in several biological systems like S-adenosyl-L-methionine dependent methyl-transferases[25] and α-glucosidase inhibitors.[24] Similarly, charge assisted halogen bonds have been described in halonium salts forming two charge assisted halogen bonds with anions[26] or Lewis bases[27,28] opposite to the two covalent bonds.

In this manuscript we report a combined Cambridge Structural Database (CSD)[29] and DFT study (PBE1PBE-D3/def2-TZVP) to analyse the existence and relevance of charge assisted PnBs in crystal structures and analyse their energetic features in some model compounds. Since we use several halophosphonium salts (X_4P^+, X = F, Cl, Br and I), we also analyse

[a] Serveis cientificotècnics, University of Balearic Islands, E- 07122, Palma, Spain
[b] Departament de Química, Universitat de les Illes Balears, Crta de Valldemossa km 7.5, 07122 Palma de Mallorca (Baleares), Spain

†Electronic Supplementary Information (ESI) available: cartesian coordinates of all optimized complexes and salts see DOI: 10.1039/x0xx00000x

its competition with charge assisted HaBs. In particular, we have compared charge assisted PnBs and HaBs by analysing the X-ray structures present in the CSD and also by computing the energetic and geometric features of two families of complexes, using halophosphonium tetraborate salts as pnicogen/halogen bond donors and several Lewis bases as σ-hole acceptors (electron donors).

Results and discussion

Preliminary CSD search

We have firstly inspected the CSD searching for X-ray structures of salts containing the RX_3P^+ cationic unit (X = halogen). As starting points, we have imposed the presence of at least three halogen atoms bonded to phosphorus for three main reasons: (i) to prevent as much as possible the overcrowding around the tetrahedral pnictogen atom and (2) to prevent the possibility to establish additional noncovalent interactions with the groups bonded to P and (iii) to analyse possible competition with charge-assisted halogen bonds. The reference codes (refcodes) of the X-ray structures found in the CSD are gathered in Table 1. Unfortunately, we have not found any structure containing the RX_3P^+ fragment for X = F. Therefore, we have expanded the search to structures with the $(CH_3)_3XP^+$ fragment, that is, structures having one halogen atom and the smallest organic group to prevent as much as possible the overcrowding around the tetrahedral P-atom. We have found three structures (X = F, Cl and I) that are represented in Fig. 1.

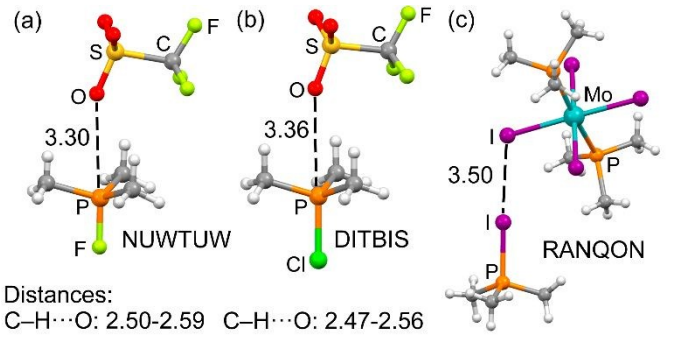

Fig. 1. X-ray solid state structures of $[(CH_3)_3XP]^+[PnF_6]^-$ (X = halogen, Pn = pnictogen) salts. (a) NUWTUW, X = F, (b) DITBIS, X = Cl and (c) RANQON, X = I. Distances in Å

It can be observed that for X = F (NUWTUW[30]) and Cl (DITBIS[31]), the O-atom belonging to the counterion is located opposite to the P–X bond at a distance that is shorter than the sum of van der Waals radii thus stablishing a charge assisted pnictogen bonding interaction. In both structures the O-atom also interacts with the H-atoms of the methyl groups thus establishing three C–H···O H-bonds that are significantly less directional than the PnB (the range of C–H···O distances is also indicated in Fig 1 for both structures). Interestingly, the O···P distance is slightly shorter in the NUWTUW[30] structure than in the DITBIS one, in agreement with the typical behaviour of σ–hole interactions. That is, with a given electron donor, the strength typically increases as the electron withdrawing ability of X increases. Remarkably, for X = I (RANQON[32]) the counterion interacts with the I-atom instead of the P-atom, thus forming a charge assisted halogen bond (HaB) instead of the PnB. A likely explanation is that the I is the best halogen bond acceptor and the worse electron withdrawing element of the series.

Other examples of charge assisted PnBs in crystal structures involving the σ-hole opposite to the F–P bond are shown in Fig. 2 including also the aforesaid NUWTUW[30] structure. Interestingly, it forms two different PnBs in the solid state (see Fig. 2a) that are highly directional and also a remarkable chalcogen bond where the F-atom is located exactly on the extension of the CF_3–S bond (179°). Fig. 2 shows two additional examples, one corresponds to the refcode ENUVEQ[33] where the O-atom of triflate interacts with the polarized P–F bond and the other one (refcode PAVSEN[34]) represents an example of intramolecular charge assisted PnB.

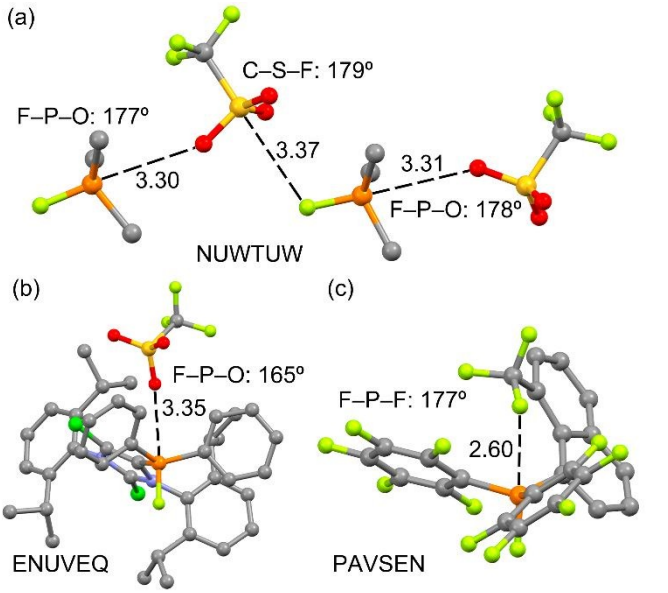

Fig. 2. X-ray solid state structures as representative example of highly directional charge assisted PnBs in R_3FP^+ salts. (a) NUWTUW, (b) ENUVEQ and (c) PAVSEN, Distances in Å

Table 1. CSD refcodes of X-ray structures with the RX_3P^+ fragment. In bold those corresponding to X_4P^+ salts

X = Cl	X = Br	X = I
BAMSAJ	**HUHHUN**	AHEMEH
LUWMIA	**YAJTOV**	**GEKNAM**
LUWNAT	**YAJTUB**	HEDGAY
SOZFUI		HEDGEC
TCXPHC10		HEDGIG
TECNOE		**HUHHOH**
		QIRZOH
		QIRZUN

We have found seventeen structures of halophosphonium cations in the CSD where the P-atom is at least bonded to three halogen atoms (six for X = Cl, three for X = Br and eight for X = I), which are indicated in Table 1. In all these structures, either the P-atom or the halogen atom exhibits strongly and directional charge assisted σ-hole interactions.

Several structures (indicated in bold in Table 1) correspond to tetrahalophosphonium salts that should present four

symmetrically distributed σ-holes, as corroborated in Fig. 3a, where the molecular electrostatic potential (MEP) surface of $[PCl_4]^+$ is represented. Two of these X_4P^+ salts (refcodes LUWNAT[35] and YAJTOV[36]) are represented in Fig. 3b and 3c and It can be observed that one atom of the counterion is indeed located opposite to one of the P–X bonds; however, the distance is very long, thus suggesting a very weak contribution of the PnB interaction. This can be due to the repulsion with the negative belts of the halogen atoms. We have compared the geometric features of these PnBs with those observed in the X-ray structure of $[AsCl_4]^+$ and $[AsBr_4]^+$ salts (Fig. 3d and 3e). Remarkably, in the case of $[AsX_4]^+$ salts, the PnBs distances O···As and F···As (in IZUXIM[37] and XALVOW,[38] respectively) are significantly shorter than the sum of their corresponding van der Waals radii and also highly directional. This result reveals the higher ability of As to establish charge assisted PnBs, in line with the typical behaviour described for conventional PnBs in trivalent pnictogen atoms.

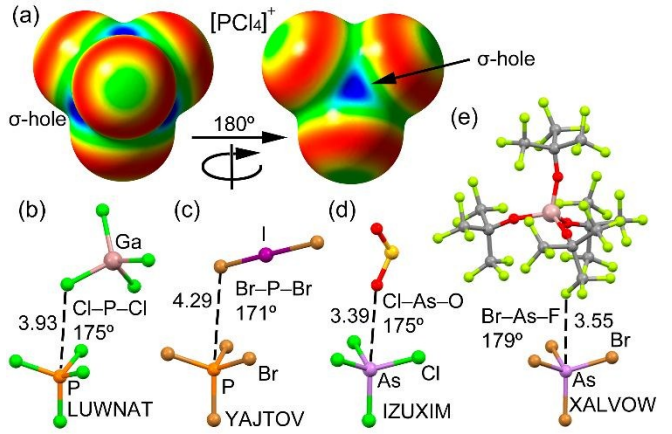

Fig. 3. (a) MEP surface (isosurface 0.001 a.u.) of $[PCl_4]^+$ is represented at the PBE1PBE/def2-TZVP level of theory. The maximum of MEP is represented in blue and the minimum in red (scale 0.15 to 0.20 Ha). (b-e) X-ray solid state structures of LUWNAT (b), YAJTOV (c), IZUXIM (d), XALVOW (e).

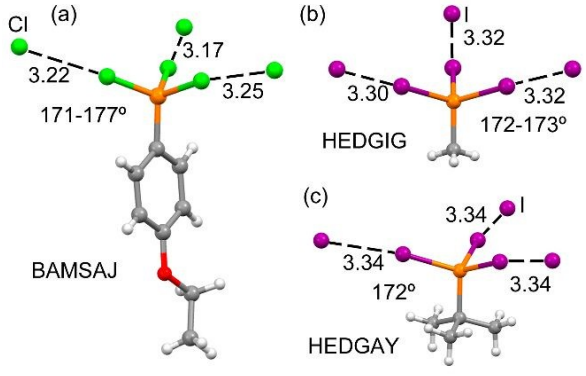

Fig. 4. X-ray solid state structures of $[P(X)_3R]^+$ cations. (a) BAMSAJ, X = Cl; (b) HEDGIG, X = I and (c) HEDGAY, X = I. Distances in Å.

The analysis of the X-ray structures of Table 1 shows that most of these compounds and specially the $[RI_3P]^+$ salts have a strong tendency to form three halogen bonds instead of the charge assisted PnB. Three illustrative examples are given in Fig. 4. In BAMSAJ,[39] the trichloro-(4-ethoxyphenyl)-phosphonium cation establishes three strongly directional interactions with the chloride counterions with Cl···Cl distances that are shorter than the sum of van der Waals radii (ΣvdW = 3.50 Å). Similarly, in both methyl-tri-iodophosphonium (HEDGIG[40]) and t-butyl-tri-iodophosphonium (HEDGAY[40]) iodide salts, three short I···I halogen bonds are established with short distances (ΣvdW = 3.96 Å), thus confirming the importance of charge assisted halogen bonds in the solid state of these compounds.

MEP surface study

With the purpose of exploring the electron density anisotropy at the phosphorus and halogen atoms in X_4P^+ salts, we have computed the molecular electrostatic potential (MEP) surfaces of the salts (compounds **1–4**, Scheme 1) as representative models of tetrahalophosphonium salts. In the first series (a) we have used $[X_4P]^+[BF_4]^-$ salts with a P–X bond pointing opposite to the $[BF_4]^-$ anion and thus suitable for establishing halogen bonding interactions at the opposite side of the anion. Another geometrical arrangement of the salt in this series has been also considered, where one B–F bond points to the P-atom of $[X_4P]^+$. However, this arrangement yields to a nucleophillic attack of one fluoride atom of $[BF_4]^-$ to the $[X_4P]^+$ cation. In the second series (b) we have used a different orientation where the P–X bond is pointing to the $[BF_4]^-$ anion, thus suitable for establishing pnictogen bonding interactions. For this series, we have also considered another geometry for the salt, where one B–F bond points to the X–P bond, thus forming a HaB interaction. However, this combination was not used in this study because it is higher in energy than the one depicted Scheme 1.

In Fig. 5 we represent the MEP surfaces of compounds **1a–4a** and in Fig. 6 those of compounds **1b–4b**. The MEP values at the σ-holes of P and X for both series "a" and "b" are summarized in Table 2. For the "a" series, the σ-hole at the P-atom is very large for X = F due to the strong electron withdrawing effect of F. Moreover, the electron density is not anisotropic at the F-atom. For the rest of halogen atoms, the distribution of electron density is anisotropic and the σ-hole slightly increases on going from Cl to I. The change is small because the MEP value is largely dominated by the global positive charge of the $[X_4P]^+$ moiety. It is interesting to highlight that the size and intensity of the σ-hole at the P–atom significantly decreases on going from the lighter to the heaviest halogen atom (see Fig. 5 and Table 2), thus strongly decreasing its ability to participate in noncovalent interactions. For the "b" series, the MEP surfaces evidence the existence of a σ-hole in X = Cl, Br and I salts with a constant value of +51 kcal/mol, thus confirming the fact that the cationic nature of the $[X_4P]^+$ fragment is masking the polarizability effect in the heavier halogen atoms. In contrast, the MEP value at the P-atom for X = F is very large ($V_{s,max}$ = 109.2 kcal/mol) and it significantly decreases on going from F to I. This analysis agrees well with the CSD results, since for X = F, pnicogen bonding interactions are common (see Fig. 2), however for phosphonium cations with heavier halogens, the PnBs are rare and HaBs predominate in the solid state. In general the MEP values are

more positive in the "b" series because the counterion $[BF_4]^-$ is located at a higher distance (longer P···B distance) due to the relative orientation of the $[X_4P]^+$ and $[BF_4]^-$ moieties.

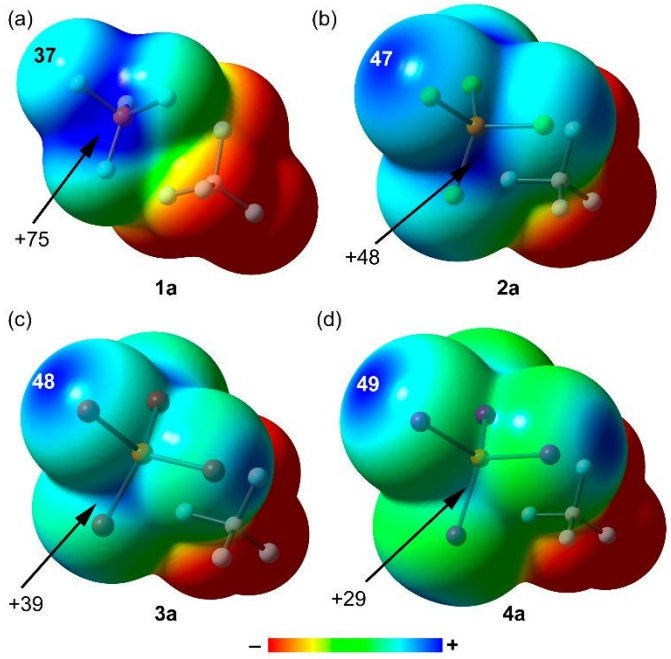

Fig. 5 MEP surfaces of compounds **1a** (a), **2a** (b), **3a** (c) and **4a** (d). Energies at selected points of the surface (0.001 a.u.) are given in kcal/mol.

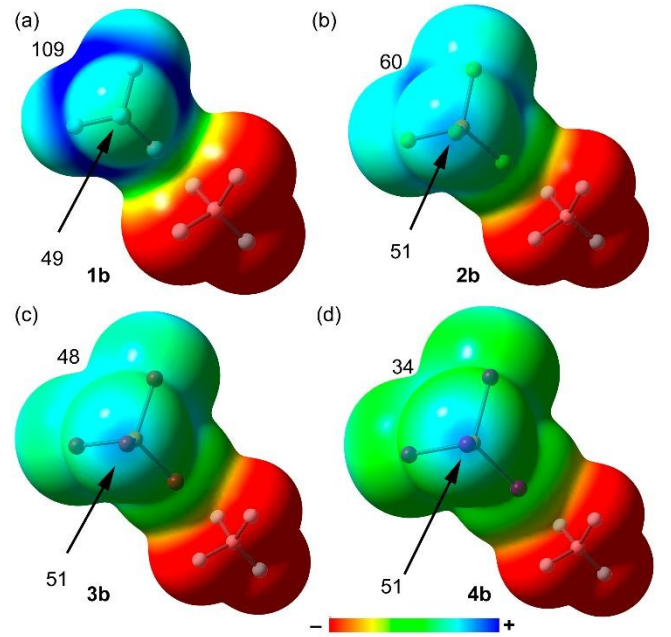

Fig. 6 MEP surfaces of compounds **1b** (a), **2b** (b), **3b** (c) and **4b** (d). Energies at selected points of the surface (0.001 a.u.) are given in kcal/mol.

Energetic analysis

The interaction energies and equilibtrium distances (PBE0-D3/def2-TZVP) for both series of complexes **5–24** (see Scheme 2) are gathered in Table 3. We have considered three neutral compounds with different donor ability (CO, HCN and NH_3) to evaluate the PnB without the large contribution of the pure electrostatic attraction between the counter-ions. In addition, we have used two different anions (SCN^- and Br^-) in order to investigate possible hypervalency in the P-atom upon complexation, especially in the fluorinated phosphonium salts that present very large values of MEP at the P-atom (see Fig. 6a).

Table 2. MEP values (in kcal·mol^{-1}) for compounds **1–4** at the PBE1PBE-D3/def2-TZVP level of theory at the halogen and P-atoms

Complex	$V_{s,X}$	$V_{s,P}$	Complex	$V_{s,X}$	$V_{s,P}$
1a	37.0	75.3	**1b**	48.9	109.2
2a	47.0	48.0	**2b**	50.8	60.8
3a	47.7	39.5	**3b**	51.4	48.3
4a	48.9	29.5	**4b**	51.4	33.8

Electron donors:
:CO HCN: H_3N: SCN^- and Br^-

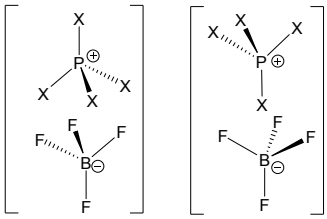

1a, X = F
2a, X = Cl
3a, X = Br
4a, X = I

1b, X = F
2b, X = Cl
3b, X = Br
4b, X = I

Scheme 1. Structures of salts **1–4** and lone pair/anionic donors.

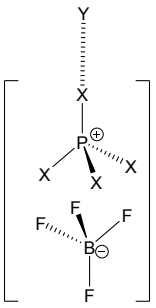

5a, X = F, Y = CO
6a, X = F, Y = HCN
7a, X = F, Y = H_3N
8a, X = F, Y = SCN^-
9a, X = F, Y = Br^-
10a, X = Cl, Y = CO
11a, X = Cl, Y = HCN
12a, X = Cl, Y = H_3N
13a, X = Cl, Y = SCN^-
14a, X = Cl, Y = Br^-

15a, X = Br, Y = CO
16a, X = Br, Y = HCN
17a, X = Br, Y = H_3N
18a, X = Br, Y = SCN^-
19a, X = Br, Y = Br^-
20a, X = I, Y = CO
21a, X = I, Y = HCN
22a, X = I, Y = H_3N
23a, X = I, Y = SCN^-
24a, X = I, Y = Br^-

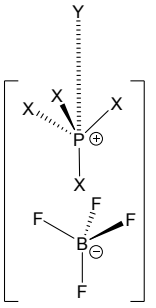

5b, X = F, Y = CO
6b, X = F, Y = HCN
7b, X = F, Y = H_3N
8b, X = F, Y = SCN^-
9b, X = F, Y = Br^-
10b, X = Cl, Y = CO
11b, X = Cl, Y = HCN
12b, X = Cl, Y = H_3N
13b, X = Cl, Y = SCN^-
14b, X = Cl, Y = Br^-

15b, X = Br, Y = CO
16b, X = Br, Y = HCN
17b, X = Br, Y = H_3N
18b, X = Br, Y = SCN^-
19b, X = Br, Y = Br^-
20b, X = I, Y = CO
21b, X = I, Y = HCN
22b, X = I, Y = H_3N
23b, X = I, Y = SCN^-
24b, X = I, Y = Br^-

Scheme 2. Two series of complexes **5** to **24** used in this work.

The interaction energies and distances for complexes **5–24** are summarized in Table 3. The energetic results indicate that the CO complexes are the weakest ones in both series and the Br^- the strongest ones. In fact, the equilibrium distances in some CO complexes are longer than the sum of van der Waals radii

(complexes **10b**, **15b** and **20b**) It is interesting to highlight that the interaction energies for the "b" series (PnBs) are larger (in absolute value) than the "a" series for X = F and X = Cl apart from complex **12** (Y = NH_3). This result strongly agrees with the MEP analysis, since the MEP at the σ-hole in the P-atom is more intense in compounds **1b** and **2b** than the σ -hole at the X-atom in compounds **1a** and **2a**. For X = Br and I, the charge assisted HaBs are stronger than the charge assisted PnBs in line with the MEP surface analysis. For the "a" series the interaction strengthens on going from X = F to X = I, as is common in HaBs[1] and for the "b" series the interaction weakens on going from F to I, in line with the lower polarization of the P–X bond in the heavier halogens. As expected, the interaction energies involving the anionic donors are stronger than those with neutral donors.

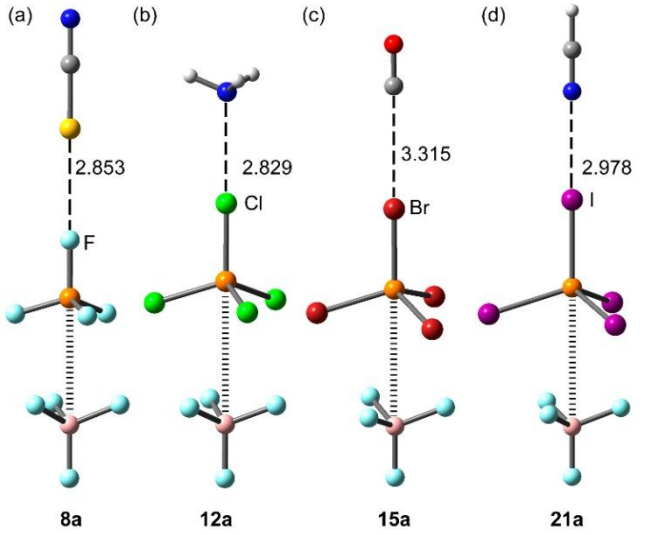

Fig. 7 PBE0-D3/def2-TZVP Optimized geometries of complexes **8a** (a), **12a** (b), **15a** (c) and **21a** (d). Distances in Å

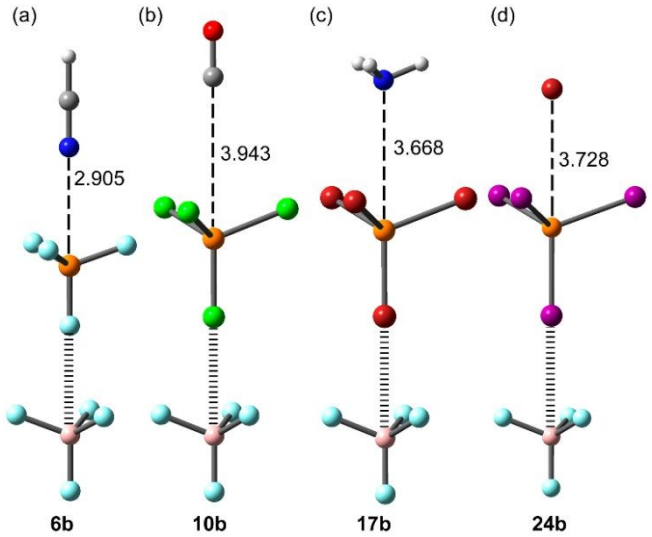

Fig. 8 PBE0-D3/def2-TZVP Optimized geometries of complexes **6b** (a), **10b** (b), **17b** (c) and **24b** (d). Distances in Å

The geometries of some representative complexes of both series are given in Figs. 7 and 8, where it can be observed that the tetrahedral geometry of the X_4P^+ unit is not changed upon complexation. However, in some complexes of the "b" series

Table 3. BSSE corrected Interaction energies (ΔE in kcal/mol), P/X···Y equilibrium distances (R, Å), electron charge density and total energy density at the bond critical point [ρ(r) and H(r), respectively, in a.u.] at the PBE0-D3/def2-TZVP level of theory for complexes **5** to **24**.

Complex	X	Y	ΔE[a]	R	ρ(r)	H(r)
5a	F	**CO**	–1.0	3.254	0.0039	0.0013
5b	F	**CO**	–4.1	3.335	0.0075	0.0009
6a	F	**HCN**	–3.5	2.923	0.0066	0.0022
6b	F	**HCN**	–11.7	2.905	0.0139	0.0012
7a	F	**NH_3**	–3.5	2.959	0.0079	0.0020
7b	F	**NH_3**	–23.6	1.972	0.1091	**–0.0895**
8a	F	**SCN^-**	–17.4	2.853	0.0110	0.0031
8b	F	**SCN^-**	–36.9	3.072	0.0145	0.0006
9a	F	**Br^-**	–24.4	2.913	0.0153	0.0023
9b	F	**Br^-**	–85.2	2.319	0.1074	**–0.0600**
10a	Cl	**CO**	–1.7	3.315	0.0067	0.0015
10b	Cl	**CO**	–2.0	3.943	0.0039[b]	0.0019
11a	Cl	**HCN**	–4.7	3.021	0.0104	0.0023
11b	Cl	**HCN**	–6.2	3.585	0.0059[b]	0.0015
12a	Cl	**NH_3**	–6.7	2.829	0.0195	0.0015
12b	Cl	**NH_3**	–6.3	3.560	0.0074[b]	0.0013
13a	Cl	**SCN^-**	–21.1	2.854	0.0216	0.0016
13b	Cl	**SCN^-**	–28.2	3.644	0.0083[b]	0.0015
14a	Cl	**Br^-**	–41.4	2.637	0.0503	*–0.0063*
14b	Cl	**Br^-**	–49.8	2.417	0.0889	**–0.0375**
15a	Br	**CO**	–2.1	3.315	0.0084	0.0014
15b	Br	**CO**	–1.4	3.907	0.0032[b]	0.0009
16a	Br	**HCN**	–5.1	3.009	0.0130	0.0019
16b	Br	**HCN**	–5.0	3.715	0.0055[b]	0.0011
17a	Br	**NH_3**	–8.6	2.729	0.0278	0.0000
17b	Br	**NH_3**	–5.2	3.668	0.0071[b]	0.0010
18a	Br	**SCN^-**	–22.7	2.844	0.0262	0.0002
18b	Br	**SCN^-**	–26.1	3.758	0.0082[b]	0.0010
19a	Br	**Br^-**	–52.6	2.567	0.0655	**–0.0138**
19b	Br	**Br^-**	–45.3	2.428	0.0862	**–0.0346**
20a	I	**CO**	–2.6	3.294	0.0112	0.0013
20b	I	**CO**	–1.8	4.108	0.0045	0.0007
21a	I	**HCN**	–6.0	2.978	0.0174	0.0015
21b	I	**HCN**	–4.0	3.854	0.0054	0.0010
22a	I	**NH_3**	–11.7	2.700	0.0355	*–0.0028*
22b	I	**NH_3**	–4.5	3.739	0.0074[b]	0.0007
23a	I	**SCN^-**	–25.1	2.855	0.0317	*–0.0021*
23b	I	**SCN^-**	–23.7	3.844	0.0086[b]	0.0009
24a	I	**Br^-**	–61.6	2.662	0.0639	**–0.0159**
24b	I	**Br^-**	–38.0	3.728	0.0118[b]	0.0006

[a]For the calculation of the interaction energies, the $[X_4P^+][BF_4^-]$ ion pair was considered as a subunit. [b]The bond paths connect the Y to the X-atoms

a nucleophilic attack of the electron rich atom to the P-atom occurs, changing from tetrahedral to trigonal pyramid. These complexes are **7b** (Y = NH_3), **9b**, **14b** and **19b** (Y = Br^-). The geometries of three of them are given in Fig. 9. It can be observed that a covalent instead of non-covalent bond is formed in these complexes, thus explaining the large interaction energies, especially for the Br^- complexes. It is

worthy to comment that in case of the NH_3 molecule, the nucleophilic attack only occurs in the complex with the $[X_4P]^+$ $[BF_4]^-$ salt, in good agreement with the MEP surface plot shown in Fig. 6a that shows a very large MEP value at the phosphorus atom's σ-hole.

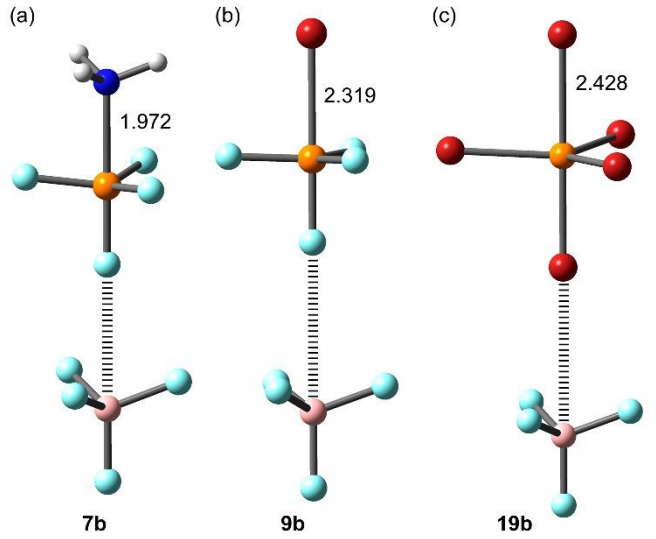

Fig. 9 PBE0-D3/def2-TZVP Optimized geometries of complexes **7b** (a), **9b** (b) and **19b** (c). Distances in Å

The characterization of the interactions in complexes **5**-**24** has been carried out using the quantum theory of "atoms-in-molecules" (QTAIM)[41]. For all complexes of the "a" series, the HaB is characterized by a bond critical point (CP) and bond path connecting the X-atom to the interacting atom of Y (marked in bold in Table 3). For the "b" series the distribution of bond CPs and bond paths is more complicated. For X = F, the PnB interaction is characterized by a bond CP and bond path interconnecting the P-atom to the electron rich atom of Y. For X = Cl, Br and I the interaction is characterized by three symmetrically equivalent bond CPs and bond paths connecting Y to three halogen atoms of the X_4P^+ unit. In these complexes, the complexation is further characterized by three ring CPs and a cage CP as a consequence of the formation of three supramolecular rings and one supramolecular cage (see Fig. 10 for a representative set of complexes of both series). The values of ρ(r) (electron charge density) at the bond CPs that characterize the HaBs in complexes **5a**-**24a** are given in Table 3. The value of ρ(r) at the bond CP correlates well with the interaction energies.[42] That is, for a given electron donor (Y) the ρ(r) values increase on going from F to I. In contrast, for the "b" series the values of ρ(r) decrease on going from X = F to X = Br≈ I, thus confirming the fact that PnBs are stronger for X = F and HaBs are stronger for X = I. In order to differentiate covalent and noncovalent interactions, we have also gathered in Table 3 the values of the total energy density [H(r)] at the bond CPs. Positive values of H(r) indicate noncovalent bonding, negative and small values of H(r) are indicative of partial covalent character, and large and negative values of H(r) along with large values of ρ(r) designate covalent bonding.[43,44] The examination of the values of H(r) in Table 3 reveal that most of the complexes are non-covalent in nature. Furthermore, halogen bonded complexes **14a**, **22a** and **23a** present partial covalent character (values in italics in Table 3) in addition to PnB complex. The QTAIM analysis also confirms the covalent character of PnBs complexes **7b**, **9b**, **14b** and **19b**, which presents trigonal bipyramid geometry around the P-atom (values in bold in Table 3) since they present large and negative values of H(r). Moreover, the HaB complexes **19a** and **24a**, that involve the anionic electron donor in combination with the heavier halogens Br and I also exhibit significant covalent character, in line with the strong σ-hole at the halogen atom (see Fig. 5).

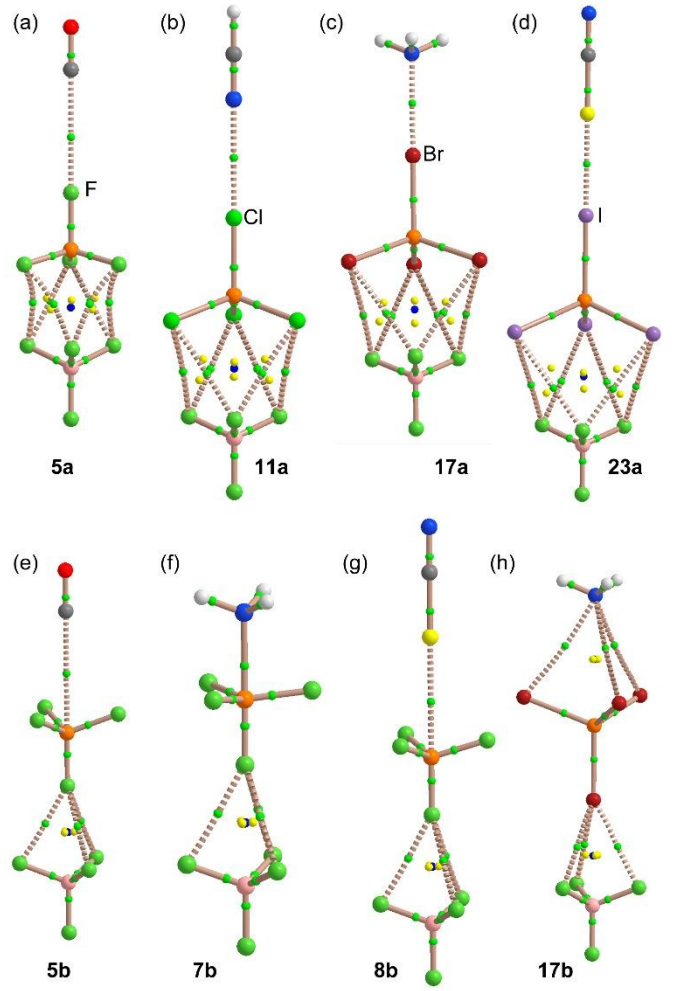

Fig. 10 QTAIM distribution of bond, ring and cage critical points (green, yellow and blue spheres, respectively) and bond paths for complexes **5a** (a), **11a** (b), **17a** (c), **23a** (d), **5b** (e), **7b** (f), **8b** (g) and **17b** (h) at the PBE1PBE-D3/def2-TZVP.

Conclusions

In conclusion, the analysis of the X-ray structures present in the CSD evidences the existence of directional charge assisted pnictogen and halogen bonds in tetravalent phosphonium, cations. The theoretical DFT calculations shows the presence of four σ-holes on the pnicogen atoms in tetrahalophosphonium

cations similar to those observed in tetrels. The X_4P^+ tetrafluoroborate salts are capable to form either charge assisted PnBs or HaBs. DFT evaluation of the interaction energies and QTAIM analysis evidence that the PnB should prevail over the HaB in fluorinated salts. Both interactions are energetically similar in chlorinated salts, however experimentally the HaB is more likely to occur due to the fact that the σ-hole at the halogen atom is significantly more accessible than that at the tetravalent Pn atom. For X = Br and I halophosphonium salts, the charge assisted HaB is stronger than the PnB as demonstrated by DFT calculations and also by the analysis of the X-ray structures of halophosphonium salts in the CSD.

Theoretical methods

The energies of all complexes included in this study were computed at the PBE0-D3/def2-TZVP level of theory. The geometries have been fully optimized imposing C_{3v} symmetry constraints by using the program Gaussian-16.[45] The interaction energy (or binding energy in this work) Δ*E*, is defined as the energy difference between the optimized complex and the sum of the energies of the optimized monomers where one of the monomers is the salt. For the calculations we have used the Weigend def2-TZVP[46,47] basis set and the PBE1PBE[48] DFT functional. The basis set superposition error (BSSE) has been corrected by using the counterpoise method.[49] The MEP (Molecular Electrostatic Potential) surfaces calculations have been computed at the same level of theory and plotted using the 0.001 a.u. isosurface as the best estimate of the van der Waals surface. The QTAIM formalism has been used to analyse the topology of the electron density,[43,44] using the same level of theory and making use of the AIMAll program.[50]

Acknowledgements

We thank the MICIU/AEI (project CTQ2017-85821-R FEDER funds) for financial support. We thank the CTI (UIB) for computational facilities.

Conflict of interest

The authors declare no conflict of interest

References

1 G. Cavallo, P. Metrangolo, R. Milani, T. Pilati, A. Priimagi, G. Resnati and G. Terraneo, *Chem. Rev*., 2016, **116**, 2478–2601.
2 P. Scilabra, G. Terraneo and G. Resnati, *Acc. Chem. Res.,* 2019*,* **52***,* 1313-1324.
3 S. Scheiner, *Acc. Chem. Res*., 2013, **46**, 280-288.
4 (a) A. Bauzá, T. J. Mooibroek and A. Frontera, *Angew. Chem. Int. Ed*., 2013, **52**, 1231 7–12321; (b) A. Bauzá, S. K. Seth and A. Frontera, *Coord. Chem. Rev*., 2019, **384**, 107-125; (c) A Bauzá, T. J. Mooibroek and A Frontera, *Chem. Commun*., 2014, **50**, 12626-12629; (d) A Bauzá, T. J. Mooibroek and A Frontera, *Chem. Eur. J*., 2014, **20**, 10245-10248.
5 (a) A. Bauzá and A. Frontera, *Angew. Chem. Int. Ed.* 2015, **54**, 7340–7343; (b) A. Bauzá and A. Frontera, *Coord. Chem. Rev*., 2020, **404**, 213112.
6 S. Grabowski, *J. Comput. Chem*, 2018, **39**, 472-480.
7 P. Politzer and J. S. Murray, *Crystals,* 2017, **7**, 212– 226.
8 J. S. Murray, P. Lane, T. Clark, K. E. Riley and P. Politzer, *J. Mol. Model.* 2012, **18**, 541–548.
9 G. Cavallo, P. Metrangolo, T. Pilati, G. Resnati and G. Terraneo, *Cryst. Growth Des*., 2014, **14**, 2697–2702.
10 (a) A. Bauzá, T. J. Mooibroek and A. Frontera, *ChemPhysChem,* 2015, **16**, 2496–2517; (b) I. Alkorta, J. Elguero and A. Frontera, *Crystals*, 2020, **10**, 180.
11 C. B. Aakeroy, D. L. Bryce, G. R. Desiraju, A. Frontera, A. C. Legon, F. Nicotra, K. Rissanen, S. Scheiner, G. Terraneo, P. Metrangolo and G. Resnati, *Pure. Appl. Chem*., 2019, **91**, 1889–1892.
12 (a) J. Y. C. Lim and P. D. Beer, *Chem.* 2018, **4**, 731– 783; (b) P. Scilabra, G. Terraneo and G. Resnati, *J. Fluorine Chem.,* 2017, **203**, 62–74.
13 M. Marín-Luna, I. Alkorta and J. Elguero, *J. Phys. Chem. A*, 2016, **120**, 648–656.
14 D. Mani and E. Arunan, *Phys. Chem. Chem. Phys*., 2013, **15**, 14377–14383.
15 (a) D. J. Pascoe, K. B. Ling and S. L. Cockroft, *J. Am. Chem. Soc*. **2017**, *139*, 15160–15167; (b) S. Scheiner, *Chem. Eur. J*. **2016**, *22*, 18850–18858.
16 E. Alikhani, F. Fuster, B. Madebene and S. J. Grabowski, *Phys. Chem. Chem. Phys*. **2014**, *16*, 2430-2442.
17 S. Moaven, M. C. Andrews, T. J. Polaske, B. M. Karl, D. K. Unruh, E. Bosch, N. P. Bowling and A. F. Cozzolino, *Inorg. Chem*., 2019, **58**, 16227-16235.
18 M. Yang, M. Hirai and F. P. Gabbaï, *Dalton Trans*., 2019, 48, 6685-6689.
19 L. M. Lee, M. Tsemperouli, A. I. Poblador-Bahamonde, S. Benz, N. Sakai, K. Sugihara and S. Matile, *J. Am. Chem. Soc*., 2019, **141**, 810-814.
20 P. Vieira, M. Q. Miranda, I. Marques, S. Carvalho, L.-J. Chen, E. N. W. Howe, C. Zhen, C. Y. Leung, M. J. Spooner, B. Morgado, O. A. B. Cruz e Silva, C. Moiteiro, P. A. Gale and V. Félix, *Chem. Eur. J*., 2020, **26**, 888-899.
21 M. Yang, D. Tofan, C.-H. Chen, K. M. Jack and F. P. Gabbaï, *Angew. Chem. Int. Ed*., 2018, **57**, 13868– 13872.
22 U. Adhikari and S. Scheiner, J. Phys. Chem. A, 2014, 118, 3183−3192.
23 S. Scheiner, *J. Phys. Chem. A* 119, 9189−9199.
24 B. Galmés, A. Juan-Bals, A. Frontera and G. Resnati, *Chem. Eur. J*., 2020, **26**, DOI: 10.1002/chem.201905498.
25 R. J. Fick, G. M. Kroner, Binod Nepal, R. Magnani, Scott Horowitz, R. L. Houtz, S. Scheiner and R. C. Trievel, *ACS Chem. Biol*. 2016, **11**, 748−754.
26 (a) L. Catalano, G. Cavallo, P. Metrangolo, G. Resnati and G. Terraneo, *Top. Curr. Chem*., 2016, **373**, 289–310; (b) G. Cavallo, J. S. Murray, P. Politzer, T. Pilati, M. Ursini and G. Resnati, *IUCrJ,* 2017, **4**, 411–419.
27 M. Ochiai, Y. Nishi, S. Goto, M. Shiro and H. J. Frohn, *J. Am. Chem. Soc*., 2003, **125**, 15304–15305.
28 M. Ochiai, T. Suefuji, K. Miyamoto, N. Tada, S. Goto, M. Shiro, S. Sakamoto and K. Yamaguchi, *J. Am. Chem. Soc*., 2003, **125**, 769–773.
29 C. R. Groom, I. J. Bruno, M. P. Lightfoot and S. C. Ward, *Acta Cryst*., 2016, **B72**, 171-179.
30 S. S. Chitnis, A. P. M. Robertson, N. Burford, J. J. Weigand and R. Fischer, *Chem. Sci*., 2015, **6**, 2559.
31 J. J. Weigand, N. Burford, A. Decken and A. Schulz, *Eur. J. Inorg. Chem*., 2007, **2007**, 4868.
32 S. Maria, F. Stoffelbach, J. Mata, J.-C. Daran, P. Richard and R. Poli, *J. Am. Chem. Soc*., 2005, **127**, 5946.

View Article Online
DOI: 10.1039/D0CE00220H

33 K. Schwedtmann, R. Schoemaker, F. Hennersdorf, A. Bauzá, A. Frontera, R. Weiss and J. J. Weigand, *Dalton Trans*., 2016, **45**, 11384.
34 I. Mallov, T. C. Johnstone, D. C. Burns and D. W. Stephan, *Chem. Commun*., 2017, **53**, 7529.
35 J. J. Weigand, N. Burford, R. J. Davidson, T. S. Cameron and P. Seelheim, *J. Am. Chem. Soc*., 2009, **131**, 17943.
36 D. Hausmann, R. Köppe, S. Wolf, P. W. Roesky and C. Feldmann, *Dalton Trans*., 2016, **45**, 16526.
37 P. Bertocco, C. Bolli, J. Derendorf, C. Jenne, A. Klein and K. Stirnat, *Chem. Eur. J*., 2016, **22**, 16032.
38 M. Gonsior and I. Krossing, *Dalton Trans*., 2005, **34**, 1203.
39 D. Mootz, W. Poll, H. Wunderlich and H.-G. Wussow, *Chem. Ber*., 1981, **114**, 3499.
40 W.-W. du Mont, V. Stenzel, J. Jeske, P. G. Jones, A. Sebald, S. Pohl, W. Saak and M. Batcher, *Inorg. Chem*., 1994, **33**, 1502.
41 R. F. W. Bader, *Chem Rev*., 1991, **91**, 893–928.
42 A. Bauzá and A. Frontera, *ChemPhysChem*, **2020**, *21*, 26-31.
43 R. F. W. Bader, M. T. Carroll, J. R. Cheeseman and C. Chang, *J. Am. Chem. Soc*., 1987, **109**, 7968–7979.
44 R. F. W. Bader, Atoms in Molecules, A Quantum Theory, Clarendon, Oxford, 1990.
45 Gaussian 16, Revision C.01, M. J. Frisch, G. W. Trucks, H. B. Schlegel, G. E. Scuseria, M. A. Robb, J. R. Cheeseman, G. Scalmani, V. Barone, G. A. Petersson, H. Nakatsuji, X. Li, M. Caricato, A. V. Marenich, J. Bloino, B. G. Janesko, R. Gomperts, B. Mennucci, H. P. Hratchian, J. V. Ortiz, A. F. Izmaylov, J. L. Sonnenberg, D. Williams-Young, F. Ding, F. Lipparini, F. Egidi, J. Goings, B. Peng, A. Petrone, T. Henderson, D. Ranasinghe, V. G. Zakrzewski, J. Gao, N. Rega, G. Zheng, W. Liang, M. Hada, M. Ehara, K. Toyota, R. Fukuda, J. Hasegawa, M. Ishida, T. Nakajima, Y. Honda, O. Kitao, H. Nakai, T. Vreven, K. Throssell, J. A. Montgomery, Jr., J. E. Peralta, F. Ogliaro, M. J. Bearpark, J. J. Heyd, E. N. Brothers, K. N. Kudin, V. N. Staroverov, T. A. Keith, R. Kobayashi, J. Normand, K. Raghavachari, A. P. Rendell, J. C. Burant, S. S. Iyengar, J. Tomasi, M. Cossi, J. M. Millam, M. Klene, C. Adamo, R. Cammi, J. W. Ochterski, R. L. Martin, K. Morokuma, O. Farkas, J. B. Foresman and D. J. Fox, Gaussian, Inc., Wallingford CT, 2016.
46 F. Weigend, R. Ahlrichs, *Phys. Chem. Chem. Phys.* **2005**, *7*, 3297–3305.
47 F. Weigend*, Phys. Chem. Chem. Phys.* **2006**, *8*, 1057–1065.
48 C. Adamo, V. Barone, *J. Chem. Phys*., **1999**, *110*, 6158-6169.
49 S. F. Boys and F. Bemardi, *Mol. Phys*. **1970**, *19*, 553.
50 AIMAll (Version 17.11.14), T. A. Keith, TK Gristmill Software, Overland Park KS, USA, (aim.tkgristmill.com), 2013.

View Article Online
DOI: 10.1039/D0CE00220H

This manuscript combines a search in the Cambridge Structural Database and DFT calculations to analyse the existence and importance of charge assisted pnictogen and halogen bonds in halophosphonium salts.